PHYSICAL REVIEW B **92**, 180410(R) (2015)

Observation of the orbital quantum dynamics in the spin-$\frac{1}{2}$ hexagonal antiferromagnet $Ba_3CuSb_2O_9$

Yibo Han,[1,2] Masayuki Hagiwara,[1,*] Takehito Nakano,[3] Yasuo Nozue,[3] Kenta Kimura,[4] Mario Halim,[4] and Satoru Nakatsuji[4,5]

[1]*Center for Advanced High Magnetic Field Science, Graduate School of Science, Osaka University, 1-1 Machikaneyama, Toyonaka, Osaka 560-0043, Japan*

[2]*Wuhan National High Magnetic Field Center, Huazhong University of Science and Technology, Wuhan 430074, China*

[3]*Graduate School of Science, Osaka University, 1-1 Machikaneyama, Toyonaka, Osaka 560-0043, Japan*

[4]*Institute for Solid State Physics, University of Tokyo, 5-1-5 Kashiwanoha, Kashiwa, Chiba 277-8581, Japan*

[5]*PRESTO, Japan Science and Technology Agency (JST), 4-1-8 Honcho Kawaguchi, Saitama 332-0012, Japan*

(Received 3 March 2015; published 16 November 2015)

We have studied orbital dynamics in the spin liquid candidate $Ba_3CuSb_2O_9$ using multifrequency electron-spin resonance. We prepared two high-quality single crystals. The crystal with a slight copper deficiency shows a structural phase transition at around 200 K due to the cooperative Jahn-Teller effect, accompanied with orbital ordering. In contrast, the crystal with almost perfect stoichiometry shows no orbital ordering down to the lowest temperature of 1.5 K. Dramatic change in the g factor anisotropy as a function of frequency and temperature demonstrates orbital quantum fluctuations at a nearly constant time scale of ~100 ps below 20 K, evidencing the emergence of an orbital liquid state in this quantum spin liquid compound.

DOI: 10.1103/PhysRevB.92.180410 PACS number(s): 75.10.Kt, 71.70.Ej, 75.25.Dk, 76.30.−v

Extensive work on various quantum spin liquid candidates has revealed that dynamic spin state may emerge close to 0 K in Mott insulators with frustrated interactions between the spins [1]. The question arises whether an analogous state is possible if additional degrees of freedom are present. In the case of orbital degeneracy, theoretical investigations revealed various types of quantum liquids [1–6]. However, the experimental realization of such states is still a challenge [7–10]. For a strongly correlated system composed of orbital-degenerated $3d$ transition ions (such as Cu^{2+}, Mn^{3+}, Cr^{2+}) in an octahedral cubic crystalline field, it is commonly known that the orbital degrees of freedom are mostly quenched by a *Jahn-Teller* (JT) effect where the JT transition occurs accompanied by crystal symmetry lowering and orbital long-range ordering at a fairly high temperature, a few thousand Kelvin, which is at least one order of magnitude higher in energy than the magnetic *exchange* interaction [11].

An exception was found for the hexagonal (6H) perovskite quantum spin liquid candidate: $Ba_3CuSb_2O_9$ (BCSO) [12,13]. In this material, a weakly connected honeycomb-based network of JT active CuO_6 octahedra face sharing with JT inactive SbO_6 rigid octahedra allows the energy scales of the JT and exchange interaction to become comparable in strength. Various measurements have revealed that the hexagonal BCSO exhibits neither magnetic long-range order nor cooperative JT transition [13–15]. The absence of orbital long-range order allows the studies on the formation of quantum spin and/or orbital liquid state in this material.

A key question is to identify the nature of the spin and orbital dynamics in BCSO, that is, whether spatial or temporal orbital disorders exist at low temperatures. For orbital dynamics, two distinct scenarios are possible: (I) static JT distortions appear locally, forming a glass type of orbital freezing, and realizing a rare case of random-singlet state [16,17]; (II) the distortions are dynamical, with a finite tunneling rate between the orbital-vibronic states at the local minima of an effective potential describing the JT coupling in the octahedra—the so-called dynamical JT effect [13,14,18,19]. This may lead to a quantum orbital liquid state. If the latter is true, the characteristic frequency of the dynamic JT distortions must be higher than 10^{10} Hz according to our previous K-band electron spin resonance (ESR) and extended x-ray absorption fine structure (EXAFS) observations [13]. The specific heat, neutron scattering, muon spin, and nuclear magnetic resonance measurements did not confirm the above scenarios, probably because the time scales in these measurements are very different from the time scale of the orbital fluctuations, and further because the imperfect hexagonal polycrystalline samples complicated the analysis [13,16].

To this end, we succeeded in preparing two kinds of high-quality single crystals of $Ba_3Cu_{1-x}Sb_{2+x}O_9$ with distinct structural behaviors [14]. One, named the "orthorhombic sample" with slight copper deficiency [$x = 0.042(1)$], shows a structural transition at about 200 K between a high-temperature hexagonal ($P6_3/mmc$) and low-temperature orthorhombic ($Cmcm$) phases, exhibiting a cooperative JT transition. The other, named "hexagonal sample," with almost perfect Sb/Cu stoichiometry ($x < 0.003$) remains hexagonal at all experimental temperatures, serving as the first copper oxide without the cooperative JT transition. Here we chose the multifrequency ESR measurement technique to investigate these samples, because its dynamic range could be extended to the high-frequency region to resonantly detect the spin and orbital magnetism simultaneously.

Let us first present the X-band ESR results at the electromagnetic wave frequency $\nu_{EM} \sim 9$ GHz, the lowest frequency available with our instrument. Distinct behaviors in the angular-dependent ESR spectra are observed for the orthorhombic [Fig. 1(a)] and hexagonal [Fig. 1(b)] samples at 2.4 K. For further discussion, we derived the g factor, ESR intensity, and linewidth from the fitting of the curves using field-derivative multiple or single Lorentzian functions (see Supplemental Material [20]).

The g factors of the orthorhombic sample clearly show anisotropic behavior due to static JT distortions [Fig. 1(c)].

*hagiwara@ahmf.sci.osaka-u.ac.jp

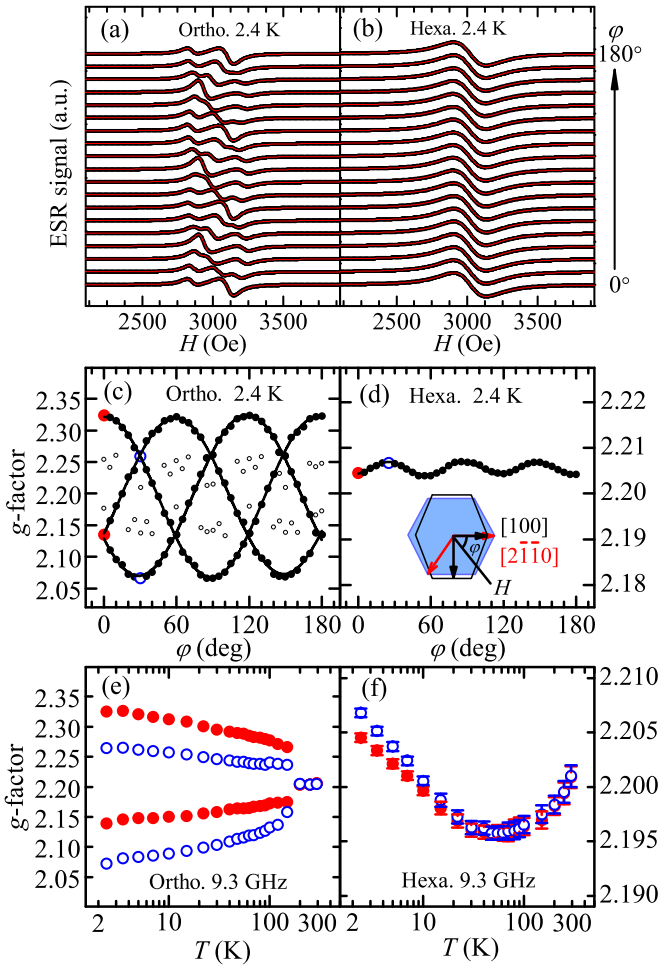

FIG. 1. (Color online) X-band ESR results measured at 9.3 GHz. (a) ESR curves of the hexagonal sample (Hexa.) for external magnetic fields rotating in ab plane at $T = 2.4$ K, (b) ESR curves for the orthorhombic sample (Ortho.) with the same setting. (c,d) In-plane g-factor anisotropy obtained from the fits of the curves in (a,b); solid lines are fits to the data by the sinusoidal function; inset of (d) defines the rotating angles φ. (e,f), Temperature-dependent g factors at $\varphi = 0°$ and 30°. Note that the g-factor scale is much different between (c,e) and (d,f).

When the magnetic field was rotated in the ab plane, three main branches with the period of 180° were observed, all branches shifted by 60° from one another, indicating the formation of three kinds of CuO_6 domains with orthorhombic elongation along the respective three Cu-O bond directions. The characteristic g factors along two long and four short Cu-O bonds are estimated as $g_{\parallel} = 2.41(1)$ and $g_{\perp} = 2.08(1)$ (see Supplemental Material [20]), which are standard values known for a strong static JT distortion in a CuO_6 octahedron [21]. On heating, a transition of the in-plane g factor from anisotropic to isotropic was observed at ∼200 K [Fig. 1(e)], confirming the cooperative JT transition.

For the hexagonal sample, however, even the lowest-temperature (2.4 K) ESR curves in Fig. 1(b) retain a perfectly symmetric Lorentzian line shape (Supplemental Material [20]). It is more striking that the g factor is almost isotropic (with a tiny sixfold symmetry) along the in-plane

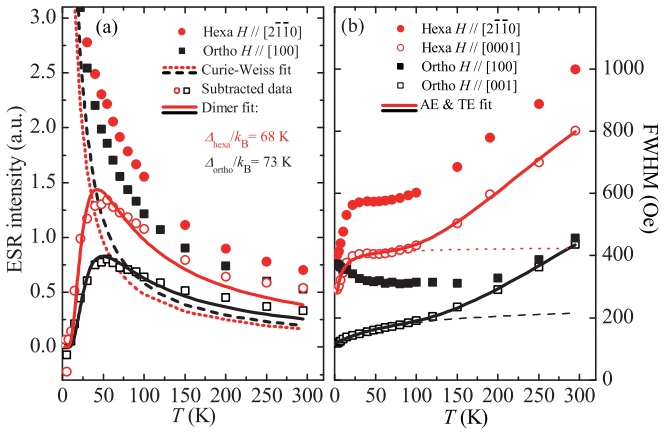

FIG. 2. (Color online) (a) ESR intensities for the hexagonal and the orthorhombic samples measured at 9.3 GHz. The "dimer" components are extracted by subtracting the "Curie-Weiss" components (low-temperature fit) from the total intensity. The obtained Weiss temperatures are nearly 0 K for both samples. The expression of dimer fittings is Eq. (S5) in the Supplemental Material SM5 [20]. (b) ESR linewidths for both samples along the a and c axes. Solid lines are the total fits, and broken lines are the anisotropic exchange fits.

directions as shown in Figs. 1(d) and 1(f), revealing the absence of cooperative JT distortion. This is unprecedented for a cupric single crystal at such a low temperature. The in-plane g factor anisotropy at $T > 20$ K [Fig. 1(f)] is totally smeared out similarly to the case of the orthorhombic sample at $T > 200$ K [Fig. 1(e)], which is most likely due to the thermally activated dynamic JT effect for the electrons coupled with the vibronic excited states [22,23].

Concerning spin and orbital dynamics, we have investigated the X-band ESR intensity and linewidth. The ESR intensities in Fig. 2(a) show similar behavior for both samples, which are proportional to the static susceptibilities [24]. At low temperatures Curie-Weiss behavior is shown for both samples, which can be attributed to about 14% "orphan spins" in the hexagonal sample, and 18% in the orthorhombic one. Subtracting the Curie-Weiss component, the remaining ESR intensity data can be fitted with a formula for the "dimer" model in which the singlet ground state and the triplet excited one are separated by the gap energy ∼70 K [23,25]. The behavior indicates that most copper spins form singlet dimers below the exchange interaction scale $J/k_B \sim 50$ K [16].

More information about the couplings of the spin, orbital, and lattice could be obtained from the ESR linewidth [full width at half maximum (FWHM)] as shown in Fig. 2(b). Both samples show a linewidth broadening with increasing temperature except for the low-temperature region of the orthorhombic sample along the [100] direction. The linewidth is much broader in the hexagonal sample than in the orthorhombic one, and a plateau (temperature-independent region) appears for the hexagonal sample, while not for the orthorhombic one. The anisotropic exchange interaction and the thermal effect may determine the ESR linewidth broadening: $\mathrm{FWHM} = K_{AE}\exp[-C_1/(T + C_2)] + K_{TE}\exp(-\Delta_{ESR}/k_B T)$ [26]. By fitting the FWHM data along the c axis for both samples

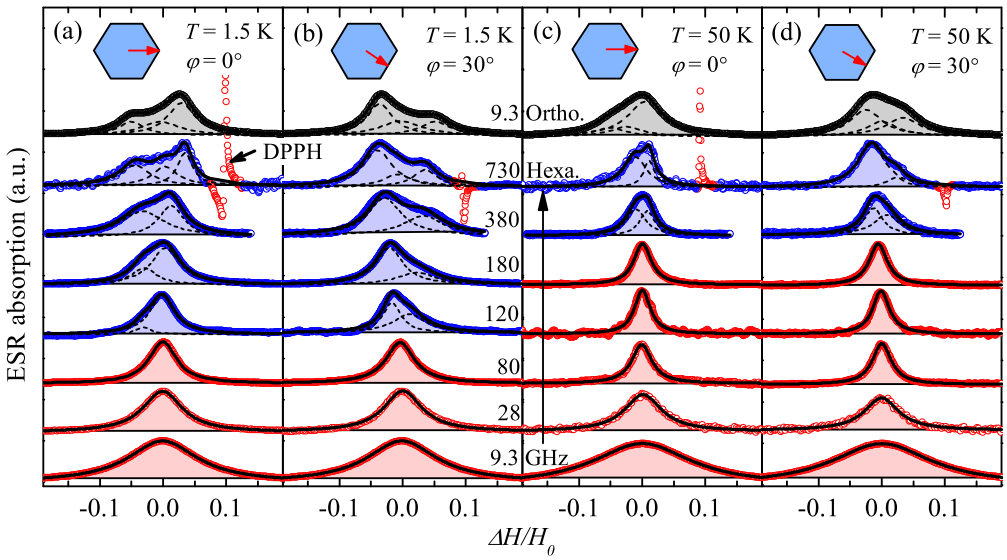

FIG. 3. (Color online) Multifrequency ESR absorption spectra. (a) $\varphi = 0°$, $T = 1.5$ K; (b) $\varphi = 30°$, $T = 1.5$ K; (c) $\varphi = 0°$, $T = 50$ K; (d) $\varphi = 30°$, $T = 50$ K. The electromagnetic wave frequency ν_{EM} varies from 9.3 to 730 GHz for the hexagonal sample. The spectra of the orthorhombic one at $\nu_{EM} = 9.3$ GHz are shown on top. $\Delta H/H_0 = (H-H_0)/H_0$, $H_0 = h\nu_{EM}/(g_1\mu_B)$, $g_1 = 2.2$. The sharp peaks at $\Delta H/H_0 \approx 0.1$ for $\nu_{EM} = 730$ GHz are the signals of DPPH (2,2-diphenyl-1-picrylhydrazyl, $g = 2.0036$). Open circles show the data, and broken and solid curves are the multipeak Lorentzian fits and the total fits, respectively.

with this equation and extracting the coefficients and the parameter values, we have found that the coefficient K_{AE} for the hexagonal sample is twice as large as that of the orthorhombic one. In contrast, the coefficients K_{TE} for both samples are similar, and the energy gaps are evaluated to be $\Delta_{ESR}/k_B = 444$ K for the hexagonal sample and $\Delta_{ESR}/k_B = 568$ K for the orthorhombic one, indicating a similar thermal fluctuation at high temperatures.

The above X-band ESR results suggest a low-temperature orbital ordering in the orthorhombic sample and the orbital fluctuations in the hexagonal one (Supplemental Material [20]). However, more convictive evidence is necessary for corroborating that this is caused by temporal orbital fluctuating rather than spatial orbital disordering. High-frequency, high-field ESR spectroscopy which covers the frequencies of 10^{10}–10^{12} Hz could be a key experiment to delineate the possible orbital dynamics. The dynamic orbital fluctuations should manifest themselves as a crossover from an isotropic to an anisotropic line shape with increasing frequency due to two kinds of mechanisms. (I) The snapshot effect: When the period of the electromagnetic wave is much longer than the time scale of orbital tunneling τ, a motional narrowed and isotropic ESR signal can be observed. On the contrary, when $1/\nu_{EM} \ll \tau$, the magnetic moment become "slowly motional," and consequently, the ESR line shape would approach that of the static JT distortion [23]. (II) Quenching of orbital quantum fluctuations under high magnetic fields [22,23]: Due to spin-orbit coupling, the magnetic field and the distortions are coupled via the anisotropic g factor. A magnetic field therefore acts as a local strain. If the potential energy of this strain—which is proportional to $g_2\mu_B H$, where $g_2 = g_{||} - g_1$, and g_1 is the average of the g-values (Supplemental Material [20])—overcomes the dynamic energy due to tunneling between the local minima, the orbitals will freeze and static JT distorted ESR spectra are expected.

Significantly, our high-frequency ESR results are found consistent with the above predictions. Figure 3 shows that the line shapes of the ESR absorption curves are clearly ν_{EM} dependent. In particular, the spectra become deformed from a symmetric Lorentzian curve when ν_{EM} exceeds a critical value: $\nu_C \sim 80$ GHz at 1.5 K [Figs. 3(a) and 3(b)], and $\nu_C \sim 180$ GHz at 50 K [Figs. 3(c) and 3(d)]. Notably, the ESR line shape at $\nu_{EM} = 730$ GHz (resonance field $H_0 = 23.7$ T for the average g value $g_1 = 2.2$) for the hexagonal sample is almost the same as the orthorhombic sample's case at 9.3 GHz, providing a high-frequency "snapshot" of the dynamic JT effect. Figure 2(a) shows that at 50 K, a temperature comparable to the spin gap, the ESR probes all the Cu sites. Therefore, the observed crossover confirms that the dynamic JT effect is a *bulk* effect.

We also note that our results clearly rule out the exchange splitting effect (ESE) [27], the other popular mechanism for the frequency-dependent crossover in ESR. Within the ESE scenario, one would assume that the local copper sites are in an orbital glass state and the exchange energy between the orphan spins is $J'/k_B = \Delta g\mu_B H_0 \sim 0.5$ K ($\Delta g = g_{||} - g_\perp = 0.32$ at the highest frequency, and $H_0 = 26.0$ kOe is the resonance field at $g_1 = 2.2$ and $\nu_C = 80$ GHz). However, the two following facts dispel this possibility: Firstly, when plotted as a function of $\Delta H/H_0$, the single Lorentzian linewidth decreases with increasing frequency at $\nu_{EM} < \nu_C$, which is opposite to the tendency expected for the ESE scenario [27]. Secondly, ν_C shifts to higher frequencies on heating (see Fig. 3), which is also opposite to the tendency expected for the ESE: ν_C would decrease because the exchange interaction would become weaker as the lattice expands [13]. Instead, the broad linewidth at low frequencies can be naturally understood as the results of dynamic mixing of the g tensor, namely, the low-frequency snapshot; the observed increase of ν_C with temperature can be understood by the

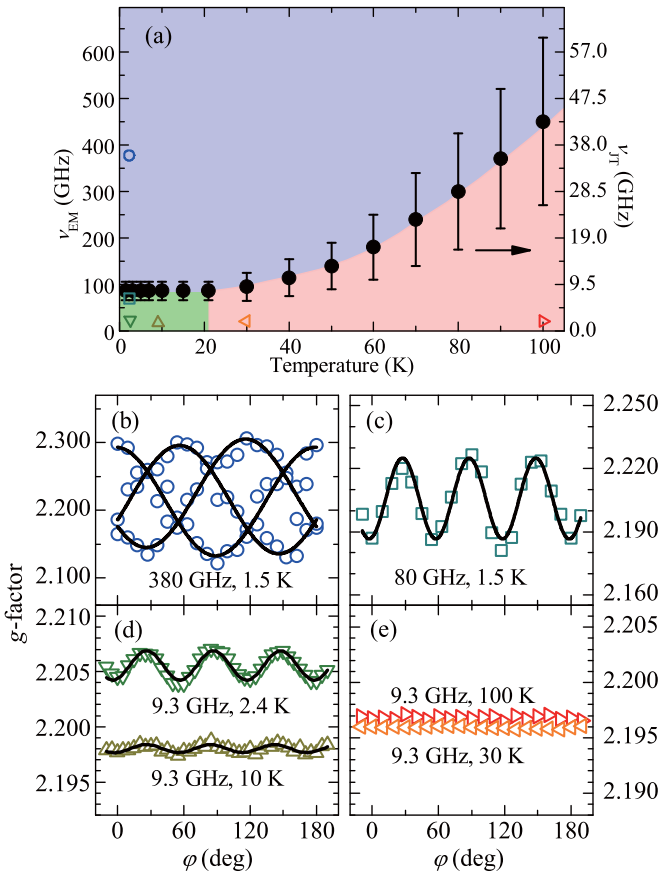

FIG. 4. (Color online) (a) Temperature dependence of the Jahn-Teller frequency (ν_{JT}). (b) Twofold symmetric g factor at $\nu_{EM} = 380\,\text{GHz}$, $T = 1.5\,\text{K}$. (c) Sixfold symmetric g factors at $\nu_{EM} = 80\,\text{GHz}$, $T = 1.5\,\text{K}$. (d) Tiny sixfold symmetric g factors at $\nu_{EM} = 9.3\,\text{GHz}$, obtained at $T = 2.4$ and 10 K. (e) Isotropic g factor at $\nu_{EM} = 9.3\,\text{GHz}$, obtained at $T = 30$ and 100 K. The experimental conditions (frequencies and temperatures) for (b–e) are shown in (a) as corresponding symbols.

fact that the orbital tunneling speeds up due to thermal fluctuations.

Thus, the dramatic change may well come from the dynamic orbital fluctuations. Using the single-ion approximation [28], we estimate the characteristic frequency of the dynamic JT effect ν_{JT} by the relation $\nu_{JT} = \nu_C g_2/g_1 \approx 0.095^*\nu_C$ (Supplemental Material [20]). As shown in Fig. 4(a), ν_{JT} systematically decreases on cooling, indicating the suppression of thermal orbital fluctuations. However, when the temperature gets lower than 20 K, ν_{JT} levels off at a constant value $\sim$10 GHz, suggesting that the orbital quantum tunneling has the time scale of about 100 ps. The temperature dependence of ν_{JT} defines the three essentially different regimes: (i) At the high-frequency, low-temperature limit, the g factor becomes as anisotropic as the orthorhombic sample's case with the static distortion as shown in Fig. 4(b). This identifies the strength of dynamic JT distortion as being comparable with that of the static JT effect, consistent with the previous EXAFS results [13]. (ii) At the low-frequency, high-temperature limit, the fully isotropic g factor due to thermal orbital fluctuations is shown in Fig. 4(e). (iii) In the low-frequency, low-temperature "quantum tunneling" region, the sixfold anisotropy of the g factor [Fig. 4(c)] was observed at $\nu_{EM} \leqslant 80\,\text{GHz}$ and $T \leqslant 20\,\text{K}$.

This emergent sixfold g factor anisotropy cannot be understood simply based on the theory for the single-ion dynamic JT effect [28,29]. Is it the fingerprint of a spin-orbital entangled state, where Cu spins form fluctuated singlet dimers which drive the dynamical Jahn Teller effect? Or is it just coming from the quantum tunneling between the orbital minima within a single ion? Various theoretical models have been developed for the BCSO: the electron-vibronic effects are emphasized in Refs. [18,19], while in Ref. [30], the importance of the coupling between the Cu spins on the honeycomb lattice and the decorating sites is stressed. It remains to be seen if these theories are compatible with our experimental findings, including the explanation of the behavior of the orphan spins, especially since we observe the same type of orbital fluctuations in the bulk and on the orphan sites.

To conclude, our multifrequency ESR measurements have identified two regimes for the dynamical Jahn-Teller effect, in addition to the cooperative Jahn-Teller effect, as a function of temperature and magnetic field. Most notably, the characteristic frequency of the orbital fluctuation below 20 K in the hexagonal BCSO remains finite and temperature independent. Together with the six-fold symmetry of the g factor, this indicates disordered orbitals with strong quantum fluctuations, forming a quantum orbital liquid. This is a sharp contrast with the static JT effect and orbital ordering observed in the orthorhombic BCSO. Together with the previous X-ray and Raman examinations [14], this orbital liquid is realized not only at orphan spin sites, but also at bulk spin site throughout all the temperature measured. Additional experiments such as infrared optical spectroscopy may further confirm this point. Finally, it is interesting to note that the frequency-dependent ESR curves in Fig. 3 are analogous to those of free spins "swimming" in a liquid solution in the biochemical "spin labels" [31], which offers a classical image of the ESR response from the orphan spins itinerating in the bulk orbital liquid.

We thank H. Sawa, S. Ishihara, Y. Wakabayashi, C. Broholm, N. Katayama, K. Kuga, and J. Nasu for discussions, K. Penc for critical reading of the manuscript and useful suggestions, and T. Kida and T. Fujita for the assistance in the pulsed high-field ESR experiments. This research is partly supported by Grants-in-Aid for Scientific Research (Grants No. 242440590 and No. 25707030), the Global COE Program (Core Research and Engineering of Advanced Materials and Interdisciplinary Education Center for Materials Science, Grant No. G10), both from the MEXT, Japan, by PRESTO of JST, Japan, and by the Natural Science Foundation of China (Grant No. 11104097). The use of the facilities of the Materials Design and Characterization Laboratory at the Institute for Solid State Physics, The University of Tokyo, is gratefully acknowledged. Some of these studies were done under a Foreign Visiting Researcher Program in the Center for Quantum Science and Technology under Extreme Conditions (KYOKUGEN).

[1] L. Balents, Nature **464**, 199 (2010).
[2] L. F. Feiner, A. M. Oleś, and J. Zaanen, Phys. Rev. Lett. **78**, 2799 (1997).
[3] S. Ishihara, M. Yamanaka, and N. Nagaosa, Phys. Rev. B **56**, 686 (1997).
[4] F. Vernay, K. Penc, P. Fazekas, and F. Mila, Phys. Rev. B **70**, 014428 (2004).
[5] P. Corboz, M. Lajkó, A. M. Läuchli, K. Penc, and F. Mila, Phys. Rev. X **2**, 041013 (2012).
[6] J. Chaloupka and A. M. Oleś, Phys. Rev. B **83**, 094406 (2011).
[7] Y. Tokura and N. Nagaosa, Science **288**, 462 (2000).
[8] A. Krimmel, M. Mücksch, V. Tsurkan, M. M. Koza, H. Mutka, and A. Loidl, Phys. Rev. Lett. **94**, 237402 (2005).
[9] M. V. Mostovoy and D. I. Khomskii, Phys. Rev. Lett. **89**, 227203 (2002).
[10] R. Fichtl, P. Lunkenheimer, J. Hemberger, V. Tsurkan, and A. Loidl, J. Non-Cryst. Solids **351**, 2793 (2005).
[11] K. I. Kugel and D. I. Khomskii, Sov. Phys. Usp. **25**, 231 (1982).
[12] H. D. Zhou, E. S. Choi, G. Li, L. Balicas, C. R. Wiebe, Y. Qiu, J. R. D. Copley, and J. S. Gardner, Phys. Rev. Lett. **106**, 147204 (2011).
[13] S. Nakatsuji, K. Kuga, K. Kimura, R. Satake, N. Katayama, E. Nishibori, H. Sawa, R. Ishii, M. Hagiwara, F. Bridges, T. U. Ito, W. Higemoto, Y. Karaki, M. Halim, A. A. Nugroho, J. A. Rodriguez-Rivera, M. A. Green, and C. Broholm, Science **336**, 559 (2012).
[14] N. Katayama, K. Kimura, Y. Han, J. Nasu, N. Drichko, Y. Nakanishi, M. Halim, Y. Ishiguro, R. Satake, E. Nishibori, M. Yoshizawa, T. Nakano, Y. Nozue, Y. Wakabayashi, S. Ishihara, M. Hagiwara, H. Sawa, and S. Nakatsuji, Proc. Natl. Acad. Sci. USA **112**, 9305 (2015).
[15] Y. Ishiguro, K. Kimura, S. Nakatsuji, S. Tsutsui, A. Q. R. Baron, T. Kimura, and Y. Wakabayashi, Nat. Commun. **4**, 2022 (2013).
[16] J. A. Quilliam, F. Bert, E. Kermarrec, C. Payen, C. Guillot-Deudon, P. Bonville, C. Baines, H. Luetkens, and P. Mendels, Phys. Rev. Lett. **109**, 117203 (2012).
[17] K. V. Shanavas, Z. S. Popović, and S. Satpathy, Phys. Rev. B **89**, 085130 (2014).
[18] J. Nasu and S. Ishihara, Phys. Rev. B **88**, 094408 (2013).
[19] J. Nasu and S. Ishihara, Phys. Rev. B **91**, 045117 (2015).
[20] See Supplemental Material at http://link.aps.org/supplemental/10.1103/PhysRevB.92.180410 for additional information on the sample preparation and measurements, and additional data and analyses.
[21] R. Englman, in *The Jahn-Teller Effect in Molecules and Crystals* (Wiley-Interscience, London, 1972), Chap. 6, p. 190.
[22] F. S. Ham, in *Electron Paramagnetic Resonance*, edited by S. Geschwind (Plenum Press, New York, 1972), Chap. 1, p. 14.
[23] I. B. Bersuker, Coord. Chem. Rev. **14**, 357 (1975).
[24] A. Abragam and B. Bleaney, *Electron Paramagnetic Resonance of Transition Ions* (Clarendon, Oxford, 1970).
[25] M. Hagiwara, Y. Narumi, K. Kindo, T. Nishida, M. Kaburagi, and T. Tonegawa, Physica B **246-247**, 234 (1998).
[26] D. V. Zakharov, J. Deisenhofer, H.-A. Krug von Nidda, P. Lunkenheimer, J. Hemberger, M. Hoinkis, M. Klemm, M. Sing, R. Claessen, M. V. Eremin, S. Horn, and A. Loidl, Phys. Rev. B **73**, 094452 (2006).
[27] H. Abe, K. Ôno, I. Hayashi, J. Shimada, and K. Iwanaga, J. Phys. Soc. Jpn. **9**, 814 (1954).
[28] I. B. Bersuker, Soviet Phys. JETP **17**, 836 (1963).
[29] M. C. M. O'Brien, Proc. R. Soc. **281**, 323 (1964).
[30] A. Smerald and F. Mila, Phys. Rev. B **90**, 094422 (2014).
[31] P. P. Borbat, A. J. Costa-Filho, K. A. Earle, J. K. Moscicki, and J. H. Freed, Science **291**, 266 (2001).